Integrated shape and material selection for single and multi-performance criteria

Jasveer Singh, Vahid Mirjalili, Damiano Pasini *

Department of Mechanical Engineering, McGill University, 817 Sherbrooke Street West, Montreal, Canada H3A 2K6

ARTICLE INFO

ABSTRACT

A shape and material selection method, based on the concept of shape transformers, has been recently introduced to characterize the mass efficiency of lightweight beams under bending and shear. This paper extends this method to deal with the case of torsional stiffness design, and generalize it to single and multi-crieria selection of lightweight shafts subjected to a combination of bending, shear, and torsional load. The novel feature of the paper is the useful integration of shape and material to model and visualize multi-objective selection problems. The scheme is centered on concept selection in structural design, and hinges on measures that govern the shape properties of a cross-section regardless of its size. These measures, referred as shape transformers, can classify shapes in a way similar to material classification. The procedure is exemplified by considering torsional stiffness as a constraint. The performance charts are developed for single and multi-criteria to visualize in a glance the whole range of cross-sectional shapes for each material. Each design chart is explained with a brief example.

© 2011 Published by Elsevier Ltd.

1. Introduction

In structural design, the most common objectives pertain to mass, axial stiffness, flexural stiffness, and torsional stiffness. Several strategies, developed in the past, are currently used to design and optimize the geometry of a structural concept with respect to these objectives. Such methods generally involve a large amount of computation time, because they often resort to techniques that require repetitive use of numeric analyses and simulations. Most of them are effective especially when they are applied at the detailed design stage, where a structural concept is already selected and the optimization search is restricted only to certain variables [1–4]. To overcome these limitations, the selection at the preliminary stage of design is often based on performance indices and design charts. A number of models for lightweight design were proposed for given loading requirements. For example, Shanley [5] examined columns under compression and introduced a minimum weight criterion based on a shape parameter governing the efficiency of alternative shapes. Cox [6] expressed performance of beams under compression and bending by the ratio of yield stress to the density of a material. In 1980s, Parkhouse [7] defined the *material dilution* factor, or *sparsity*, to compare different structural concepts to an equivalent reference cross-section. Based on these premises, Ashby, the world-renowned authority in material selection, introduced a pioneering methodology to search the best material for a given application [8–10]. Huang and Gibson [11] identifies the optimum

cross-sectional shape for various materials by analyzing the maximum shape factor limited either by local buckling or by yielding. Along the lines of Ashby's material indices, Rakshit and Ananthasuresh [12] derived new design indices for the trusses. These indices help in choosing the suitable material for any design of a truss. Warner [13] introduced constraint indices that aids in co-selecting shape and material for spatially limited components. Thomas in his work [14] introduced material architecture indices for composite multi-functional materials. These indices provide a useful metric for ranking composite design configurations. All the above mentioned works did not consider integrating shape and material for multi-objective structural optimization, the focus of this paper.

More recently, another method has been introduced to study the effects of material and shape of structures subjected to geometric constraints [15–17]. This paper extends such a method to limited torsion stiffness design for single and multi-objective selection. The main objective of the paper is to generalize the shape transformer approach for a multi-criteria selection involving bending, shear and torsion. The paper starts by reviewing the fundamentals of the method which is used in Section 3 to formulate the performance indices for a number of general cases including single and multi-objective design problems. To demonstrate the method in these scenarios of selection, Section 4 and 5 examine problems with prescribed torsional stiffness.

2. Methodology

The shape transformer approach introduced for material and structural selection hinges on the premise of systematically decoupling the effect of shape from that of size. Demonstrated for single-

* Corresponding author.
 E-mail addresses: Jasveer.singh@mail.mcgill.ca (J. Singh), vahid.mirjalili@mail.mcgill.ca (V. Mirjalili), damiano.pasini@mcgill.ca (D. Pasini).

objective optimization [15,16], this decoupling eases the way a change in geometry of the cross-section can be handled to visualize the optimum solutions (Pareto front) for multi-objective selection. For a cross-section, the shape, referred as S, is the figure that fits within the rectangular envelope whose size is specified by the height and width of the cross-section (Fig. 1). The scheme used in this paper resorts to envelope multipliers and shape transformers, to quantitatively measure changes in shape and size properties of a cross-section. These are briefly introduced in the following sub-sections.

2.1. Envelope multipliers

Size changes between different cross-sections, e.g. Fig. 1a and b are measured by the envelope multipliers. The relative scaling of an arbitrary cross-section with envelope sizes B and H, relative to a reference rectangular envelope with sizes B_0 and H_0, is described by the envelope multipliers, u and v, as

$$\begin{cases} u = B/B_0 \\ v = H/H_0 \end{cases} \tag{1}$$

2.2. Shape transformers

For a given cross-section, a shape transformer (Ψ_G) of a geometric quantity G is defined by normalizing the geometric quantity G by the same geometric quantity of its envelope G_D, such that $\Psi_G = G/G_D$. The shape transformers of area (Ψ_A), bending (Ψ_I) and shear (Ψ_S) are already defined [15,16]. The shape transformer introduced in this paper is that of torsion which is defined as,

$$\Psi_{JT} = \frac{J_T}{J_{TD}} \tag{2}$$

where J_T and J_{TD} are the torsional constants respectively of the cross-section and of the envelope.

We recall here that this approach classifies shape concepts into families and classes to ease the comparison of alternative cross-sectional shapes. A shape family is identified by the name of the solid shape from which a cross-section is derived. A shape class can be regarded as a subset of a family. Discrimination among shape classes is defined by the ratio between the size of the internal opening and the external shape [16,17].

In this paper, the expressions of the shape transformers are formulated for shapes subjected to a given torsional stiffness. For this, we resort to approximated formulas [18,19] that describe the torsional constants with less than 3% error relative to experimental results. We consider common classes of two families: the rectangle and the ellipse (Table 1). In addition to these, we also consider a number of classes of shapes commonly used in structural design, e.g. circular sector, pinned shafts, cross shafts and circular segmental section.

3. Performance indices for multi-criteria selection charts

The basic procedure for co-selection of shape and material is outlined in this section through the formulation of design objectives and constraints in terms of shape transformers, envelope multipliers and material properties. Each objective is described by a performance index which measures the efficiency of a cross-section with respect to that objective. In general, we can express a performance index, P, in terms of design requirement, F, material properties, M, and geometry, G, such that

$$P = f(F, M, G) \tag{3}$$

The shape transformers allows expressing the geometry parameter, G, in terms of shape properties, S, and size properties, D, of a cross-section; hence,

$$P = f(F, M, \underbrace{S, D}_{G}) \tag{4}$$

For multi-objective selection, we first consider two performance indices, P_1 and P_2

$$P_1 = f_1(F, M, \underbrace{S, D}_{G}) \tag{5}$$

$$P_2 = f_2(F, M, \underbrace{S, D}_{G}) \tag{6}$$

For a given shape and material, and functional requirement, the above objectives and the stiffness constraint (as demonstrated in Sections 3.1 and 3.2) are only a function of size such that:

$$P_1 = f_3(u, v) \tag{7}$$

$$P_2 = f_4(u, v) \tag{8}$$

$$v = f_5(u) \tag{9}$$

These equations can be used to express a performance metric as a function of the other,

$$P_1 = f_6(P_2) \tag{10}$$

To use these equations for the development of design charts, we can follow two approaches.

The first one consists of plotting one objective versus the other using Eq. (10). This procedure allows exploring the Pareto front of optimal (non-dominated) solutions as discussed in Section 5.1; although simple, this strategy has some limitations. First, it does not visualize the relation between the objective function space and the decision space, i.e. the design variable space. Second, the change of performance with respect to any change of constraint can be difficult to estimate. Third, if more than one constraint is present, numerical optimization methods should be applied to obtain the Pareto front, a condition that vanishes our aim to gain insight through the visualization of the results of the optimization problem.
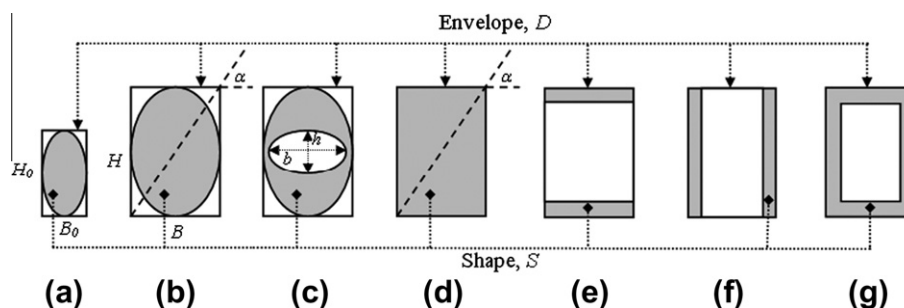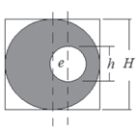

Fig. 1. The envelope (D) and the embedded shape (S).

Table 1
Shape transformers for common shapes (For all shapes, B and H is the breadth and height of the envelope, and t is the thickness).

Cross-sections	A	$\Psi_A = A/A_D$	J_T	$\Psi_{JT} = J_T/J_{TD}$	$\lambda = \Psi_{JT}/\Psi_A$
The rectangle family, closed-walled cross-sections					
	BH	1	$\dfrac{BH^3}{16}\left(\dfrac{16}{3} - 3.36\left(\dfrac{H}{B}\right) + 0.28\left(\dfrac{H}{B}\right)^5\right)$	1	1
	$2t(H+B) - 4t^2$	0 to 1	$\dfrac{2t^3(H+B-2t)}{3} + \dfrac{2t(H-t)^2(B-t)^2}{H+B-2t}$	0 to 1	1.03 to 1.77
	$2t(H+B) - 4t^2$	0 to 0.36	$\dfrac{2t(H-t)^2(B-t)^2}{H+B-2t}$	0 to 0.52	1.44 to 1.77
$B = H$	$B^2 - \pi r^2$	0.364 to 1	$32CB^4$ where $C = 1.1266 - 0.3210\dfrac{2r}{B} + 3.1519\left(\dfrac{2r}{B}\right)^2$ $-14.347\left(\dfrac{2r}{B}\right)^3 + 15.223\left(\dfrac{2r}{B}\right)^4 - 4.7767\left(\dfrac{2r}{B}\right)^5$ $\dfrac{2r}{B} \leq 0.9;\ B = H$	0.09 to 1	0.24 to 1
The rectangle family, open-walled cross-sections					
	$t(H+2B) - t^2$	0 to 0.28	$\dfrac{t^3}{3}(2B+H-2t)$	0 to 6.6×10^{-3}	0 to 0.02
	$t(H+2B) - t^2$	0 to 0.28	$\dfrac{t^3}{3}(2B+H-t)$	0 to 7.5×10^{-3}	0 to 0.02
	$t(H+B) - t^2$	0 to 0.19	$\dfrac{t^3}{3}(B+H-2t)$	0 to 4.9×10^{-3}	0 to 0.02

Table 1 (*continued*)

(square box)	$2t(H+2B)-4t^2$	0 to 0.36	$\frac{2t^3}{3}(B+H-2t)$	0 to 9.3 x10^{-3}	0 to 0.02
(channel)	$t(H+2B)-2t^2$	0 to 0.28	$\frac{t^3}{3}(2B+H-2t)$	0 to 6.6 x 10^{-3}	0 to 0.02
(two sides)	$2Bt$	0 to 0.2	$\frac{2Bt^3}{3}$	0 to 2.3 x 10^{-3}	0 to 0.01
(square + channel)	$2t(H+2B)-4t$	0 to 0.36	$\frac{2t^3}{3}(B+H-2t)$	0 to 9.3 x 10^{-3}	0 to 0.02
The ellipse family					
(filled circle)	$\frac{\pi}{4}BH$	$\frac{\pi}{4}$	$\frac{\pi}{16}\frac{B^3H^3}{B^2+H^2}$	0.7	0.9
(ring)	$\frac{\pi}{4}(BH-bh)$	$0\ to\ \frac{\pi}{4}$	$\frac{\pi}{16}\frac{B^3H^3}{B^2+H^2}(1-c^4)$	$0\ to\ 0.7$	$0.88\ to\ 1.11$
(thin ring)	$\frac{\pi}{2}t(H+B-2t)$	$0\ to\ 0.09\pi$	$\dfrac{\pi t(B-t)^2(H-t)^2}{2(B+H-2t)\left(1+0.258\dfrac{(B-H)^2}{(B+H-2t)^2}\right)}$	$0\ to\ 0.4$	$1.44\ to\ 1.77$
(eccentric) $B=H$	$\frac{\pi}{4}(H^2-h^2)$	For e=0.05H 0.16 to π/4 For e=0.15H 0.4 to π/4 For e=0.30H 0.66 to π/4	$\dfrac{\pi(H^4-h^4)}{32C}$ *where* $C=1+\dfrac{16n^2}{(1-n^2)(1-n^4)}\lambda^2+\dfrac{384n^4}{(1-n^2)^2(1-n^4)}$ $\lambda=e/D \quad n=d/D$	For e=0.05H 0.07 to 0.7 For e=0.15H 0.27 to 0.7 For e=0.30H 0.5 to 0.7	For e=0.05H 0.35 to 1.26 For e=0.15H 0.66 to 0.96 For e=0.30H 0.73 to 0.89

Table 1 (continued)

Other common shapes

$B = H$ — $\dfrac{\alpha H^2}{8}$ — 0 to 0.785 — $\dfrac{CH^4}{32}$

where $C = 0.0034 - 0.0697\left(\dfrac{\alpha}{\pi}\right) + 0.5825\left(\dfrac{\alpha}{\pi}\right)^2$
$- 0.2950\left(\dfrac{\alpha}{\pi}\right)^3 + 0.0874\left(\dfrac{\alpha}{\pi}\right)^4 - 0.0111\left(\dfrac{\alpha}{\pi}\right)^5$

$0.1 \leq \dfrac{\alpha}{\pi} \leq 2.0$

— 0 to 0.7 — 0.016 to 0.49

$B = H$

$H^2 - \left[\dfrac{H^2}{2}\left(4\sin^{-1}\left(\dfrac{a}{H}\right)\right.\right.$
$\left.- \sin\left(4\sin^{-1}\left(\dfrac{a}{H}\right)\right)\right) +$
$\dfrac{a^2}{2}\left(\pi - 2\sin^{-1}\left(\dfrac{a}{H}\right) -\right.$
$\left.\left.\sin\left(\pi - 2\sin^{-1}\left(\dfrac{a}{H}\right)\right)\right)\right]$

0.44 to 0.785

$\dfrac{CH^4}{8}$

$C = 0.784 - 0.0225\left(\dfrac{2a}{H}\right) - 1.4154\left(\dfrac{2a}{H}\right)^2 + 0.9167\left(\dfrac{2a}{H}\right)^3$

(a is the radius of the groove)

0.1 to 0.7 — 0.68 to 0.89

$B = H$

$H^2 - 4\left[\dfrac{H^2}{2}\left(4\sin^{-1}\left(\dfrac{a}{H}\right)\right.\right.$
$\left.- \sin\left(4\sin^{-1}\left(\dfrac{a}{H}\right)\right)\right) +$
$\dfrac{a^2}{2}\left(\pi - 2\sin^{-1}\left(\dfrac{a}{H}\right) -\right.$
$\left.\left.\sin\left(\pi - 2\sin^{-1}\left(\dfrac{a}{H}\right)\right)\right)\right]$

0.7 to 0.785

$\dfrac{CH^4}{8}$

$C = 0.784 - 0.0409\left(\dfrac{2a}{H}\right) - 6.2371\left(\dfrac{2a}{H}\right)^2 + 7.2538\left(\dfrac{2a}{H}\right)^3$

(a is the radius of the groove)

0.48 to 0.7 — 0.23 to 0.89

The second approach overcomes the above drawbacks, as it involves the development of a four-quadrant-performance-chart, as shown in Section 5.2 through an example of multi-objective design problem for a prescribed torsional stiffness and a geometric constraint. The strategy is to plot envelope multipliers (u, v) and objectives (P_1, P_2) through Eqs (7)–(10) onto its four axes, to visualize one curve for each combination of shape and materials in each quadrant. The four quadrants share common axis and consist of the planes: u versus v, u versus P_1, v versus P_2, and P_1 versus P_2. The first quadrant represents the decision space and the second quadrant represents the first objective function. Likewise, the fourth quadrant represents the second objective function and the third quadrant shows the feasible objective space for the given set of constraints represented in the first quadrant.

It is noteworthy that for a single-objective function, e.g. P_1, the four-quadrant-performance-chart reduces to a two quadrant-per-formance-chart, as discussed in Section 4 for torsional stiffness design. In Section 4, we also generate efficiency maps similar to those proposed for bending stiffness design [16], as they can conveniently visualize performance limits for each shape family and its classes. However, they can handle problems with only one selection criterion. The performance indices are formulated in the following sub-sections for prescribed torsional stiffness. The indices for some other common cases are given in Table 2.

3.1. Minimizing mass for torsional stiffness constrained design

For limited torsional stiffness design, we consider a shaft of length l in equilibrium under a torque T, with a twist angle, θ. The general form of the torque, T, can be written as [20],

$$T = GJ_T \frac{d\theta}{dz} - E\omega \frac{d^3\theta}{dz^3} + \frac{1}{2}EI_n \left(\frac{d\theta}{dz}\right)^3 \tag{11}$$

where GJ_T is the torsional stiffness of a bar with shear-modulus G, $d\theta/dz$ is the rate of rotation with respect to the z-axis, E is the Young's modulus, w is the warping constant, and I_n is a section property referred to as non-linear Wagner constant.

The third term in Eq. (11) is used for plastic analysis of shafts, whereas the second describes the warping effects of cross-sections. The former involves non-linear elastic torsion which rarely occurs in practice and whose effects are negligible in a small deformation regime. The latter arises in a cross-section with warping-restrained supports. The warping effect decreases with an increase of the shaft length, provided the torque is applied far from the warping-restrained end [18]. Either in the case of free warping boundary conditions on both ends, or in the case of relatively long beams with length to depth ratio of more than six [18], the last two terms in Eq. (11) are negligible. Therefore, under such conditions, the torsional stiffness of a shaft of length l can be simplified to:

Table 2
Performances indices for given design scenarios.

Design objective	Formulation of optimization problem in terms of shape transformers
Single-objective	
Minimizing mass for pure bending stiffness constrained design	Minimize $P = \frac{1}{m} = \frac{(\Psi_I E)^q}{\Psi_A \rho}$ Subject to $uv^3 = \frac{1}{(E/E_0)\Psi_I}$
Minimizing mass for shear constrained design	Minimize $P = \frac{1}{m} = \frac{1}{uv\rho\Psi_A} = \frac{G}{\rho} \cdot \frac{\Psi_S}{\Psi_A}$ Subject to $uv = \frac{1}{(G/G_0)\Psi_S}$
Minimizing mass for bending and induced shear stiffness constrained design	Minimize $P = \frac{1}{m} = \frac{1}{uv\rho\Psi_A}$ Subject to $\frac{1 - \frac{1}{(G/G_0)\Psi_S uv}}{\frac{1}{(E/E_0)\Psi_I uv^3} - 1} = \frac{10\alpha l^2 G_0}{\beta E_0}$
Minimizing mass for torsional stiffness constrained design	Minimize $P = \frac{1}{m} = \frac{(\Psi_{JT} G)^q}{\Psi_A \rho}$ Subject to $u^{1.55} v^{2.45} = \frac{1}{(G/G_0)\Psi_{JT}}$
Multi-objective	
Minimizing mass and maximizing flexural stiffness for torsional constrained design	Maximize $P_1 = \frac{1}{m} = \frac{(\Psi_{JT} G)^q}{\Psi_A \rho}$ Maximize $P_2 = 1/\left(\frac{6}{5\alpha G \Psi_S uv} + \frac{12l^2}{\beta E \Psi_I uv^3} \right)$ Subject to $u^{1.55} v^{2.45} = \frac{1}{(G/G_0)\Psi_{JT}}$
Minimizing mass and maximizing torsional stiffness for bending constrained design	Maximize $P_1 = \frac{1}{m} = \frac{(\Psi_I E)^q}{\Psi_A \rho}$ Maximize $P_2 = (0.14)G\Psi_{JT}.u^{1.55} v^{2.45}$ Subject to $uv^3 = \frac{1}{(E/E_0)\Psi_I}$
Minimizing mass and maximizing torsional stiffness for bending and induced shear constrained design	Maximize $P_1 = \frac{1}{m} = \frac{1}{uv\rho\Psi_A}$ Maximize $P_2 = (0.14)G\Psi_{JT}.u^{1.55} v^{2.45}$ Subject to $\frac{1 - \frac{1}{(G/G_0)\Psi_S uv}}{\frac{1}{(E/E_0)\Psi_I uv^3} - 1} = \frac{10\alpha l^2 G_0}{\beta E_0}$
Maximizing flexural and torsional stiffness for geometrically constrained design	Maximize $P_1 = \frac{1}{m} = \frac{1}{uv\rho\psi_A}$ Maximize $P_2 = (0.14)G\Psi_{JT}.u^{1.55} v^{2.45}$ Subject to $v = f(u)$

$$k = \frac{Tl}{\theta} = GJ_T \tag{12}$$

In torsion stiffness design, the torsional stiffness, K_{req}, is prescribed, and should be met by the candidate cross-sections. Other design requirements are usually the length and the boundary conditions of the shaft, whereas, material and geometry of the cross-section are often the variables. The torsional constraint can be expressed in terms of envelope multipliers, shape transformers, and material properties (see Appendix A), as

$$u^{1.55} v^{2.45} = \frac{1}{(G/G_0)\Psi_{JT}} \tag{13}$$

Eq. (13) allows us to plot constant stiffness lines for different combinations of shape and material on a uv plane, which is the first quadrant of the performance chart previously described and representing the decision space. Fig. 2 is an example of this chart, where three different values of $G\Psi_{JT}$ are plotted to estimate the direction in which the reference cross-section can be scaled to meet the torsional stiffness requirement. For a given combination of shape and material, arbitrary scaling of a reference cross-section is obtained by moving the upper right corner of the envelope along the relevant stiffness requirement curve. It is worthy to mention here a benefit of defining shape transformers with respect to size. The stiffness requirement curve does not change as long as the product of mate-

rial and shape properties remains the same. For example, the constant stiffness curve will remain the same if G is halved and Ψ_{JT} is doubled.

For given torsional stiffness, the performance index (pertaining to mass) of a cross-section can be expressed in terms of material, shape, and envelope multipliers as (see Appendix A),

$$P = \frac{1}{m} = \frac{(\Psi_{JT} G)^q}{\Psi_A \rho} \tag{14}$$

where q is the scaling parameter and can be expressed in terms of envelope multipliers, for $u \geqslant v$, as

$$q = \frac{\ln(uv)}{\ln(u^{1.55} v^{2.45})} \tag{15}$$

When a geometrical constraint is applied a priori to the cross-section size, u and v are known and the scaling parameter, q, is constant. The performance index is then governed by material and shape properties alone. To show the effect of the scaling parameter on material selection for a prescribed shape, three choices of material: Ti, Cu, and Mg are considered. Table 3 shows that Ti is the best choice of material for proportional scaling. However, when the design scenario imposes a height constraint, then, Mg is the best option.
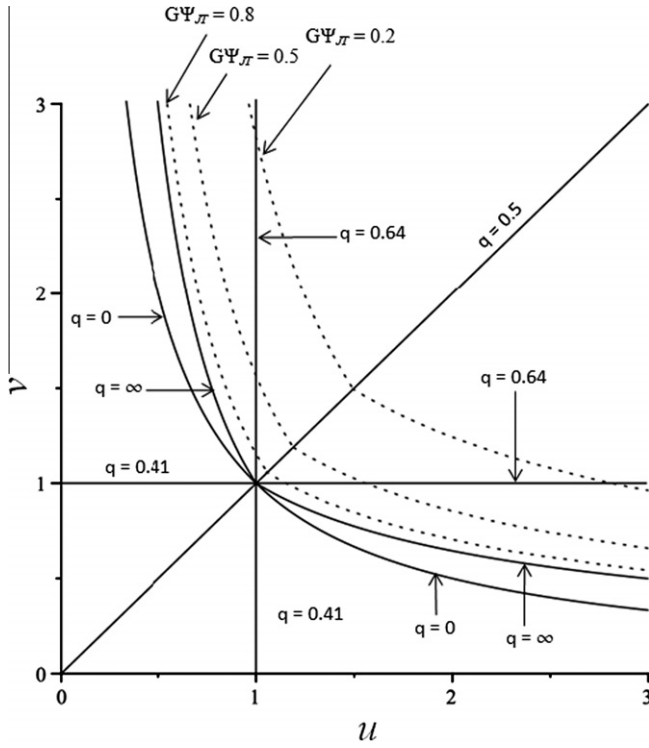
Fig. 2. Constant stiffness (torsional) curves on uv plane.

Table 3
An example to demonstrate the effect of imposing three prescribed ways of scaling candidate cross-sections.

Material	E (GPa)	G (GPa)	ρ (Mg/m³)	G/ρ	$G^{0.41}/\rho$	$G^{0.64}/\rho$
Ti	107	45	4.49	10.03	1.1	2.55
Cu	101	37.5	7.5	5	0.6	1.36
Mg	45	17	1.8	9.44	1.8	3.41

3.2. Minimizing mass and maximizing flexural stiffness for torsional constrained design

For the multi-objective case, we need two performance indices. The first index minimizing mass, as explained in Section 3.1, can be written as,

$$P_1 = \frac{1}{m} = \frac{(\Psi_{JT} G)^q}{\Psi_A \rho} \tag{16}$$

To derive the second performance index consisting maximizing the flexural stiffness, consider a cantilever beam under a point load F which can be modelled as two springs mounted in series. The combined bending and shear stiffness can be written [15] as,

$$\frac{FlK}{\alpha GA} + \frac{Fl^3}{\beta EI} \tag{17}$$

where α and β are constants dependent on the boundary and loading conditions, l is the length, A is the cross-section area, and K is the shear correction factor dependent on the shear stress distribution.

Eq. (17) represents the second objective, which in terms of shape transformers and envelope multipliers reduces to

$$P_2 = 1 \bigg/ \left(\frac{6}{5\alpha G \Psi_S u v} + \frac{12l^2}{\beta E \Psi_I u v^3} \right) \tag{18}$$

As explained in Section 3.1, the torsional constraint can be written as

$$u^{1.55} v^{2.45} = \frac{1}{(G/G_0)\Psi_{JT}} \tag{19}$$

Hence, Eqs. (16), (18), and (19) can be plotted into a four-quadrant-performance-chart, as illustrated in Section 5.2. A similar procedure can be followed for the other general multi-objective cases tabulated in Table 2.

For specific cases, the same approach can be used to formulate performance indices and constraints. For example, consider the design of a helical spring for minimum mass; the constraint is the deflection per unit load. The performance index for mass is

$$P = \frac{1}{m} = \frac{1}{u v \rho \Psi_A} \tag{20}$$

The constraint of deflection per unit length can be written as

$$\frac{FD^2}{4GJ} + \frac{F}{AG} \tag{21}$$

where F is the load, D is the outer diameter and A is the area of the cross-section.

Candidate cross-sections will be those which satisfy the constraint Eq. (21) which expressed in terms of shape transformers and envelope multipliers reduces to,

$$\frac{1 - \dfrac{1}{(G/G_0)\Psi_{JT} u^{1.55} v^{2.45}}}{\dfrac{1}{(G/G_0)\Psi_A u v} - 1} = \frac{0.56}{D^2} \tag{22}$$

The performance chart for selecting the optimum combination of shape and material for the spring can be plotted using Eqs. (20) and (22). Any additional constraints can be considered by plotting them in the first quadrant of the four-quadrant-performance chart.

4. Selection charts for single-objective case – mass minimization for torsional stiffness design

By resorting to the model presented so far, we present in this section efficiency maps and performance charts for single-objective selection in torsional constrained design. Shape efficiency maps are first introduced for selecting shape for a prescribed envelope and then for a scaled envelope. The cases of shape and material co-selection follow.

4.1. Shape selection for a prescribed envelope

Similar to bending, we introduce here the efficiency parameter for torsion stiffness design as the ratio of the shape transformer of the torsional constant Ψ_{JT} to the shape transformer of the area Ψ_A for a cross-section with prescribed size and material.

$$\lambda_{JT} = \Psi_{JT}/\Psi_A \tag{23}$$

The ranges of the efficiency parameter are listed in the last column of Table 1 for different cross-sections. The higher the value of the efficiency parameter, the lighter and stiffer in torsion is the cross-section. In bending stiffness design, the efficiency limits are independent on the envelope scaling [16,21]. In contrast for torsion, the efficiency limits are dependent on the scaling of the envelope, which is governed by the angle α (Fig. 1d). The culprit for this is that Ψ_{JT} is a function of α as opposed to Ψ_I. In most cases, such as in hollow rectangles, the performance increases when the envelope tends to be a square, i.e. $\alpha \approx 45°$, but for practical values of α the increase is less than 5%. Hence, at the conceptual stage of design, Ψ_{JT} (and, thus, efficiency parameter) could be assumed constant.
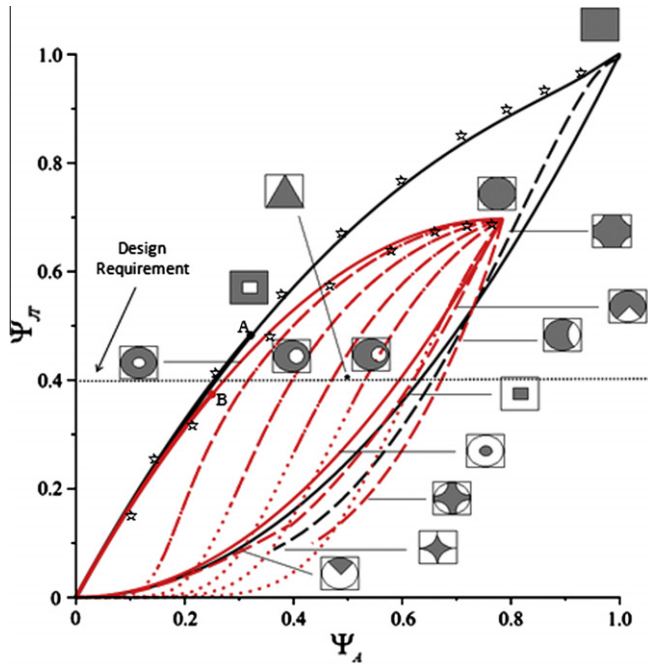
Fig. 3. Efficiency map for a prescribed envelope (closed-walled cross-sections) (numerical results from FEA are also shown).

Fig. 3 shows the efficiency map for commonly used shape and families, each characterized by specific efficiency limits. For closed-wall cross-section, all classes of the ellipse and rectangle families fall within the limiting curves of the hollow rectangular envelope (solid black lines). On the other hand, open-walled cross-section falls outside this domain due to a lower efficiency. As an example, consider a design requirement of 0.4, the intersections of the horizontal dotted line and the curves show that the hollow rectangular shape is the lightest among the candidate
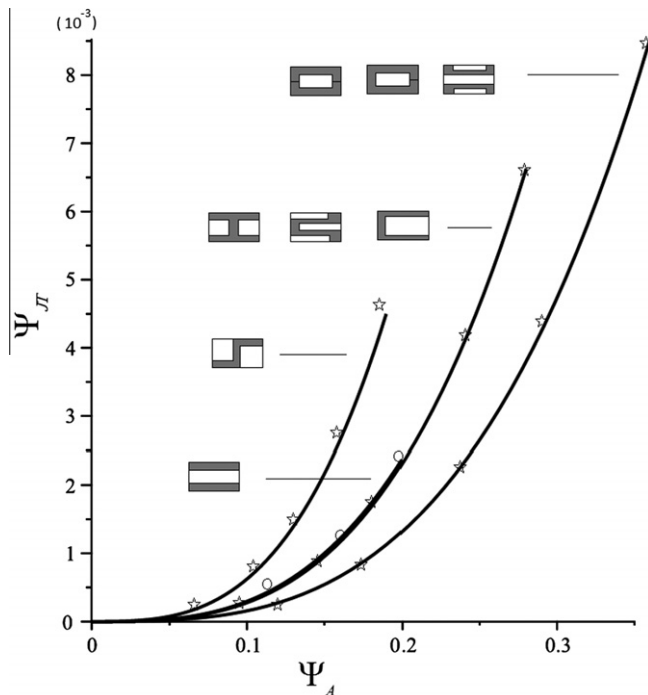
cross-sections shown in Fig. 3. Furthermore, the map shows that as the eccentricity of hollow ellipse increases, its efficiency decreases, as shown by the rightward shift of the curves. The lower solid red and black curves are theoretical limiting cases that describe a cross-section with a stiff core material coated by a material with lower, almost negligible shear-modulus, G, e.g. foam. As expected, the efficiency curves show that stiff core materials with low shear-modulus coating are not efficient in torsion stiffness design.

Points A and B specify the bounds of the validity range of the thin-walled theory which pertain to cross-section with thickness ten times smaller than the minimum dimensions of a cross-section. Thin-walled theory predictions estimate values of the torsional constant from the origin to point A and B with an error of less than 2% with respect to thick-walled theory estimations.

Fig. 4 illustrates the efficiency curves for open cross-sections in limited torsion stiffness design. The range of the shape transform-
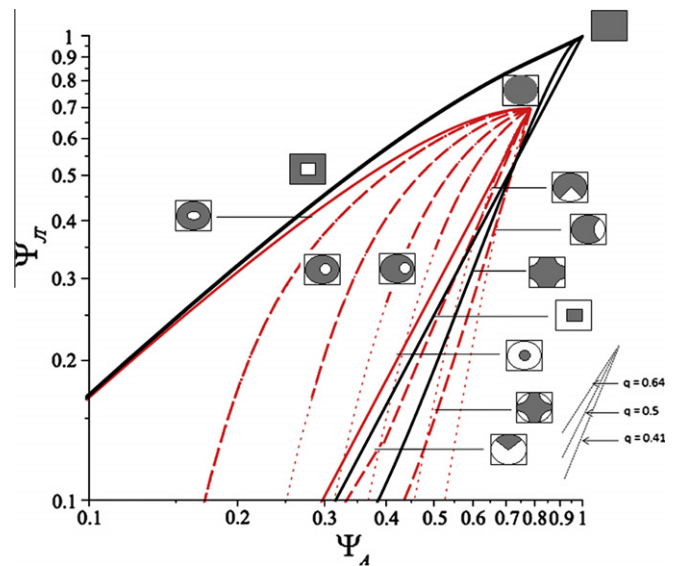
Fig. 5. Efficiency map for scaled cross-sections (closed-walled cross-sections), logarithmic-scale.

Fig. 4. Efficiency map for a prescribed envelope (open-walled cross-sections) (numerical results from FEA are also shown).
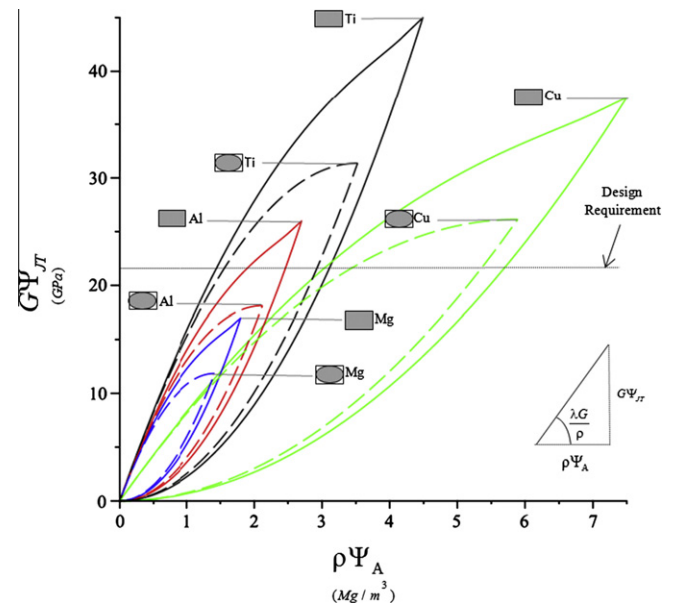

Fig. 6. Material and shape co-selection for four typical materials (prescribed envelope).

ers for the torsional constant is around 10^{-3}. Unlike in bending where an I-beam is one of the most efficient shapes, the map shows that for a given torsional stiffness, the I-beam is quite inefficient. It could also be seen that the Z-beam concept is the best choice, because it provides the highest value of the efficiency parameter, λ_{JT}.

4.2. Shape selection for scaled cross-sections

Similar to Fig. 3, Fig. 5 is a logarithmic-scale chart for the selection of scaled cross-sections. Due to the decoupling of shape and size, this method allows plotting guidelines for shape selection in any scaling condition. These guidelines can be obtained by taking the logarithm of the performance index;

$$\log \Psi_{JT} = \frac{1}{q} \log \Psi_A + \frac{1}{q} \log P \qquad (24)$$

Eq. (24) plotted in Fig. 5 describes an iso-performance line with slope $1/q$ and y-intercept $1/q\log P$. When the scaling direction is imposed by geometric constraints applied to the cross-section size, such as in tightly constrained structures, q is known and can be used as the slope of a selection guideline. Given the slope, the y-intercept will directly give the performance of the shape in question. Thus, for a given scaling, the higher the y-intercept; the lighter the cross-section.

In Fig. 5, iso-performance lines, which describe cross-sections with the same efficiency, are plotted for $q = 0.41$, $q = 0.5$, and $q = 0.64$ respectively for horizontal, proportional, and vertical scaling. To compare two scaled cross-sections subjected to a specific geometrical constraint q, a line with slope $1/q$ should be plotted passing through the cross-section co-ordinates, (Ψ_A, Ψ_{JT}). The one with higher y-intercept, $1/q \log P$, performs better than the others. As depicted in Fig. 5, for horizontal scaling, elliptical cross-section performs better than the rectangular one. However, for a prescribed envelope, the opposite is true. Hence, illustrating the performance index on a logarithmic chart simplifies the selection of a scaled cross-section. It should be noted that these efficiency maps can only be used if q is constant for all the candidate shapes. To deal with cases where q can vary, performance charts explained in Section 4.4 should be used.

4.3. Co-selection of shape and material for a prescribed envelope

The efficiency maps introduced for shape selection can be extended to assist the co-selection of shape and material. This co-selection, for non-scaled cross-sections, is governed by the index;

$$P = \frac{\Psi_{JT} G}{\Psi_A \rho} = \lambda \frac{G}{\rho} \qquad (25)$$

Fig. 6 illustrates a typical example of co-selection of shape and material using efficiency maps. $(\rho\Psi_A, G\Psi_{JT})$ specify the co-ordinates of a cross-section on the chart. As an example, the materials considered in the figure are Ti, Cu, Al and Mg. For each of these, the stiffness curves for the Rectangle and the Ellipse families are plotted. The chart shows that a copper beam can meet higher stiffness requirement compared to a magnesium beam. However, when magnesium can also satisfy the stiffness requirement, it will perform better due to its higher efficiency parameter.

As another example, a stiffness requirement of 22 (GPa) is considered in Fig. 6. Aluminum, copper and titanium beams can satisfy the stiffness requirements. However, since the efficiency parameter, $\lambda G/\rho$, is the highest for the point on the solid black curve closest to the y axis; a hollow rectangular cross-section made up of titanium is the best choice.
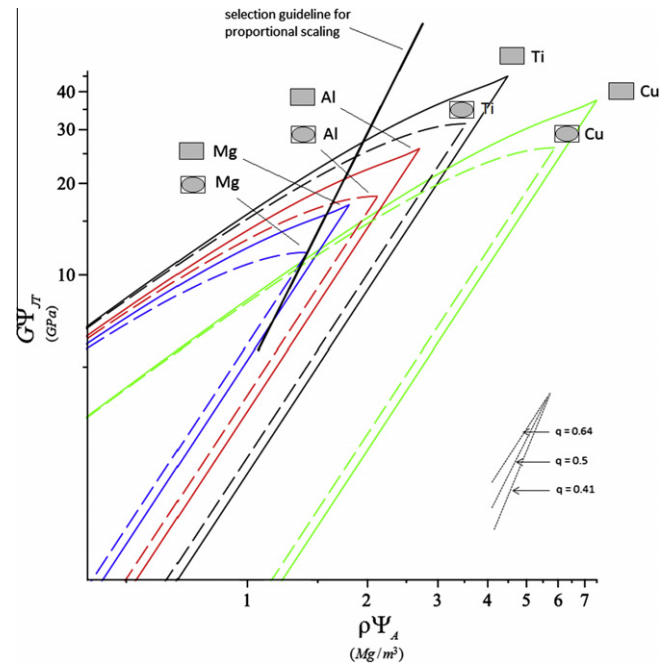

Fig. 7. Material and shape co-selection for four typical materials (horizontally, vertically, and proportionally scaled cross-sections).

4.4. Co-selection of shape and material for scaled envelope

Co-selection of material and shape for scaled cross-sections is considered in Fig. 7. For this scenario, we can rearrange the performance index in logarithmic-scale to obtain the following iso-performance lines for a given scaling condition;

$$\log G\Psi_{JT} = \frac{1}{q} \log \rho\Psi_A + \frac{1}{q} \log P \qquad (26)$$

For a given q, the higher the y-intercept, the lighter the cross-section. For instance, $q = 0.41$, $q = 0.5$, and $q = 0.64$ are plotted in Fig. 7 for horizontal, proportional, and vertical scaling, respectively. The plot shows that for proportional scaling, an elliptical cross-section made up of Magnesium is the lightest among the candidate solid cross-sections. All combinations of shape and material that lie above the selection guideline perform better than the solid magnesium ellipse.

The efficiency charts discussed above are relevant when the scaling direction (q) is constant. A complementary graphical selection method is developed here to deal with cases where scaling can be done in all directions. This is a two-quadrant-performance-chart (Fig. 8) obtained by following the description given in Section 3. The right part of the chart consists of constant stiffness curves drawn on uv plane. In the left part, the performance is plotted against the vertical envelope multiplier (or height of envelope).

Consider an example of a geometrical constraint shown in the right part of Fig. 8. The aim is to co-select shape and material. The candidate materials are steel and aluminum, and the candidate shapes are rectangle and ellipse. It can be seen from the figure that Aluminum-Rectangle scaled to point A (Fig. 8) is the most efficient followed by the Aluminum rectangular cross-section scaled to a different point B. The third best combination is the steel-ellipse which is about 15% heavier than the best possible cross-section.

The results of the mathematical model presented in this paper for torsion were compared with the numerical results obtained through finite element analysis (FEA) using ANSYS, a commercial finite element software. The validation was completed for all shape
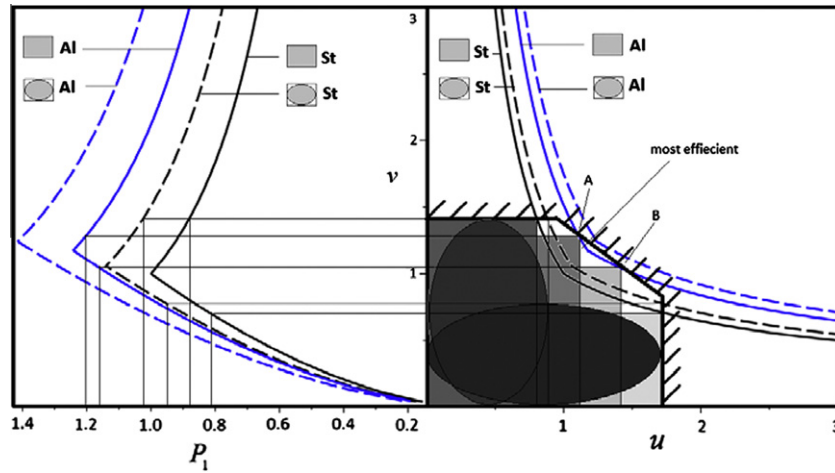
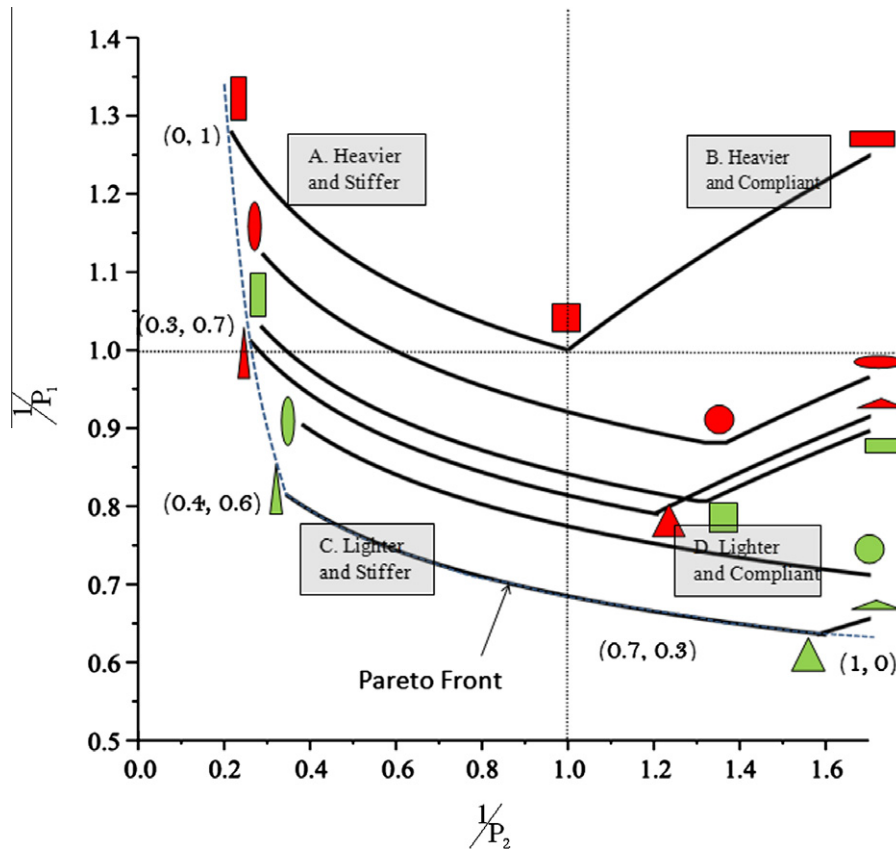**Fig. 8.** Performance chart for prescribed torsional stiffness considering a geometrical constraint.

Fig. 9. Both objectives (flexural stiffness and mass) plotted against each other for solid cross-sections (red – steel; green – aluminum).

classes listed in Table 1. To avoid crowding the maps, however, the validation points of two shape classes are included (Figs 3 and 4). Since the torsional constant is derived from the mesh, the accuracy of the torsion constant is directly proportional to the mesh size of the cross-section. The default mesh used by ANSYS yields acceptable accuracy for elastic analysis. The mesh size was set to the finest level. Concerning the boundary conditions, the cross-section is assumed to be free to warp to retrieve from ANSYS the numerical values of the warping constant given by Eq. (11). The maximum difference between the numeric and analytic results is found to be 5% which is due to the approximations made in deriving the torsional constant. Nevertheless, this accuracy is deemed acceptable,

especially for the conceptual stage of design. It is worth mentioning that shape transformers of bending and shear were previously validated [15–17].

5. Selection charts for multi-objective case – mass minimization and flexural stiffness maximization for torsional stiffness design

The fundamental difference between single and multi-objective optimization is the number of optimal solutions. In single-objective optimization, there is only one optimum solution,

whereas in multi-objective optimization, several trade-off solutions between conflicting objectives exist. Among these optimal solutions, none can be considered to be better than the other and thus are known as non-dominated solutions, namely Pareto-optimal solutions [22].

Methods to handle MOO problems can be loosely classified in two categories. Within the first one, there are classical approaches which involve specifying a priori a preference vector that scalarizes an objective vector into a single composite objective function. These are referred as preference-based methods, which are highly subjective to the user definition of a reliable preference vector that converts multi-objective optimization into a single-objective optimization yielding only one optimal solution. The second category of methods to handle MOO involves finding firstly all non-dominated solutions and then using higher level information to choose one of the obtained solutions. These methods are referred as a posteriori approaches; they are appropriate to give a broad view of the available alternatives, without the need to define a preference vector in advance.

In this paper, a posteriori approach is adopted to visualize non-dominated solutions of a MOO problem where the design variables are the geometric properties, i.e. shape and size, and the material attributes. In contrast to the penalty function method adopted by Ashby [19] for material selection, the artificial/pseudo-weight method [22] is used here as it can also capture concave Pareto front. The procedure is explained through the following example.

Consider a rod, an element that forms the basic unit of most of the complex structures. One end is assumed to be fixed to simplify the study (though it could be easily extended to a simply supported beam). The objectives are to minimize its mass and maximize its flexural stiffness while complying with given torsional stiffness and a manufacturing constraint (for example height/breadth < 3). The candidate materials are Steel and Aluminum. The shapes considered, here, are from the rectangle family, ellipse family, and triangle, since these are commonly used shapes. We formulate the MOO problem as,

$$
\left.\begin{array}{l}
\text{Minimize } \dfrac{1}{P_1} = \dfrac{\Psi_A \rho}{(\Psi_{JT} G)^q} \\[2mm]
\text{Maximize } \dfrac{1}{P_2} = \left(\dfrac{6}{5\alpha G \Psi_S u v} + \dfrac{12l^2}{\beta E \Psi_I u v^3} \right) \\[2mm]
\text{Subject to } u^{1.55} v^{2.45} = \dfrac{1}{(G/G_0)\Psi_{JT}} \\[2mm]
v < 3u
\end{array}\right\}
\tag{27}
$$

The values of α and β [18] are 1 and 3 respectively for this case. For the values of shape transformers for bending and shear, the reader is referred to [15,16], whereas the values of the shape transformers for torsion are listed in Table 1. The length of the rod is given as .032 m. The analysis is divided into two cases: first, when the envelope is allowed to scale in any direction; second, when the envelope is constrained.

5.1. Co-selection of shape and material for a freely scalable envelope

For a given combination of shape and material, the objectives and constraints are only function of the envelope multipliers (u, v). This allows plotting both objectives against each other, as explained in Section 3. Fig. 9 shows the plot for the selected candidate solid shapes and materials whereas the visualization of boundaries for shape families is illustrated separately in Fig. 9. Each point on a curve, $1/P_1 = f(1/P_2)$ represents a candidate cross-section differing in shape, size and material. The plot in Fig. 9 is divided into four sectors with respect to the baseline steel-squared cross-section at the center. The solutions in the sector C are both lighter and stiffer, thus the best. Those in the sectors A and D are better by one objective. Those in sector B are heavier and less stiff, thus the worst. To further narrow down the optimal solutions, we draw a Pareto front as a dashed line.

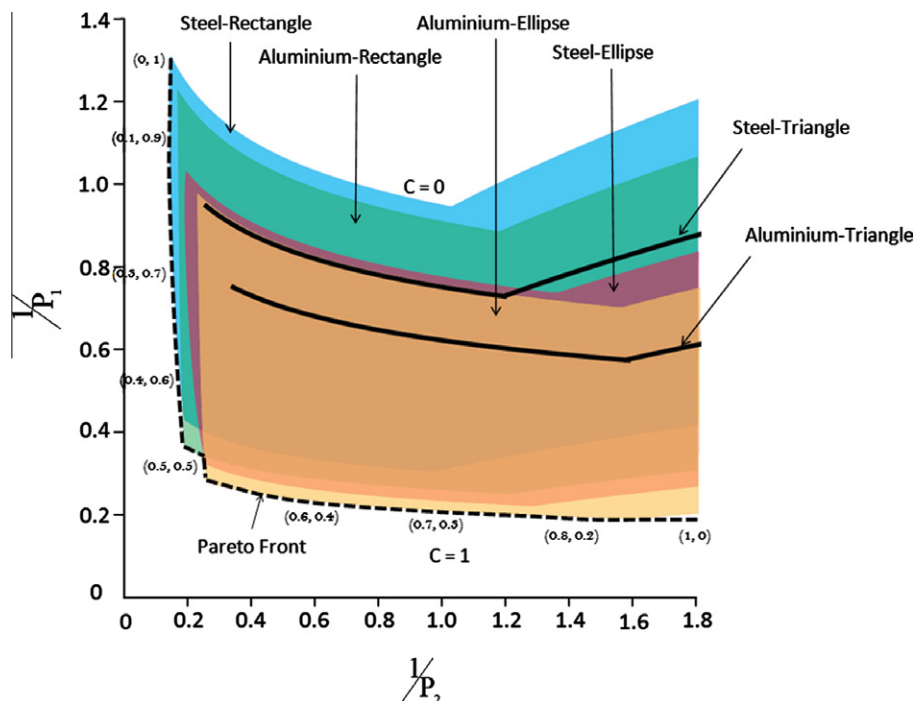**Fig. 10.** Both objectives (flexural stiffness and mass) plotted against each other for shape families. P_2 refers to flexural stiffness and P_1 to mass. As reported in Table 1, C = 0 describes solid cross-sections, which are at the upper boundaries of each shaded domain; C = 1 represents the ideal case of very thin hollow cross-sections, which represent the lower limiting curves of each shape family domain.

The solutions nearest to this front are optimal trade-off cross-sections. Although case-specific, a designer will be inclined towards the cross-sections in sector C (as demonstrated in Fig. 9) which illustrates that vertically scaled Aluminum-Triangle is the best choice.

A rational approach to select the final optimum solution from the Pareto set is to impart artificial/pseudo-weight vector to each solution. Consider, for example, the Pareto-optimal set of the vertically scaled steel rectangle (sector A), which corresponds to a 0% preference of the first objective and a 100% preference of the second objective. This preference values can be associated to pseudo-weights by assigning a weight vector $(w_1, w_2) = (0, 1)$. Likewise, this strategy can be used to assign pseudo-weight vector to each solution by estimating their location on the Pareto front. The weight factor can be written as,

$$w_i = \left(\frac{f_i^{max} - f}{f_i^{max} - f_i^{min}} \right) \bigg/ \left(\sum_{j=1}^{M} \frac{f_j^{max} - f_j}{f_j^{max} - f_j^{min}} \right) \qquad (28)$$

where f_i^{min} and f_i^{max} denote the minimum and maximum values of the ith objective function among the Pareto-optimal solutions.

When the trade-off among objectives is known, this knowledge can be used to choose one of the non-dominated solutions, which will closely match the information conveyed by the artificial weight vector. For instance, if a similar trade-off between two objectives is required, the solution closer to a weight vector (0.5, 0.5) should be chosen. In Fig. 9, this choice is illustrated by the vertically scaled Aluminum triangle. Other weight factors pertaining to the Pareto solutions are shown in brackets for the Aluminum triangle.

To handle shape families, we follow the same approach, as shown by the pseudo-weight vectors added as coordinate points on the Pareto Front of Fig. 10 for the candidate families. Whereas Fig. 9 shows the triangular cross-section to be the best among solid ones, Fig. 10 shows a Pareto front divided into three regions, each described by alternative combinations of material and shape families. In particular, the Aluminum-Rectangle part represents the optimum candidates if flexural stiffness is preferred; the Aluminum-Ellipse part if mass weighs more; and the Steel-Rectangle one if both objectives are of the same importance. In the first case, the hollow steel-rectangle family (vertical part of the Pareto Front) is the best choice closely followed by the hollow Aluminum-Rectangle. In the second case, the hollow Aluminum-Ellipse family (lower part of the Pareto Front) is the best selection followed by hollow Steel-Ellipse. In the third case where both objectives are given equal weights, the hollow Aluminum-Rectangle family (central part of the Pareto Front) is preferable. Fig. 10 helps also estimate the relative performance of thin walled cross-sections with respect to solid cross-sections. The upper boundaries of each colored-region represent solid cross-sections described by C = 0, as defined in Table 1; C = 1 are ideal cross-sections with vanishing thickness.

It is noteworthy to mention that to solve the multiobjective optimization problem, other classical approaches could have been used, as opposed to the artificial/pseudo-weight method. For example, assigning a priori weight factors to each objective is an alternative, which might have two drawbacks. First, it might not able to capture the whole Pareto Front even if a uniformly spaced set of weight vectors is assigned, as demonstrated by Deb [22]. Second, it cannot handle concave Pareto frontier.
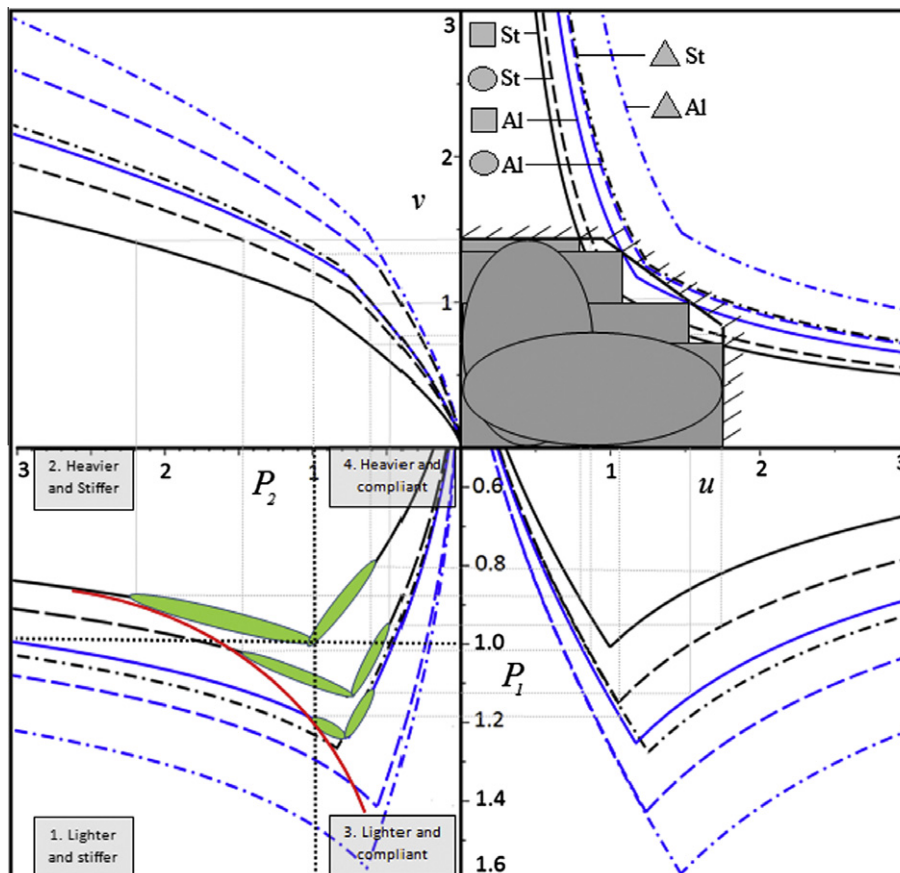

Fig. 11. Four-quadrant-performance-chart demonstrating the Pareto front (red curve).

5.2. Co-selection of shape and material for a constrained envelope

Consider a problem in which different constraints are applied to the envelope, which is not free to be scaled. For example, these geometrical constraints might be:

$$v = 1.5, \qquad\qquad 0 < u < 0.9$$
$$v = -0.82u + 2.24, \quad 0.9 < u < 1.75 \qquad\qquad (29)$$
$$u = 1.75, \qquad\qquad 0.8 < v < 0$$

To handle such a geometric constrained design, we resort to the four quadrant-performance chart (Section 3) which involves plotting the constraints on the uv plane. Regardless of the number of constraints, this approach visualizes the relation between the decision space of the design variables and the objective space of the objective functions. As explained in Section 3, the first quadrant represents the decision space in which each constraint, e.g. geometric, manufacturing, flexural stiffness, torsional stiffness, mass, strength, or/and cost, can be plotted. To plot these constraints, they need to be expressed in terms of shape transformers and envelope multipliers. This is explained with the example of a cost (of material) constraint. The total cost of a material used in a mechanical component can be written as;

$$\text{Total cost} \propto \text{mass} \times \text{cost/mass} \qquad\qquad (30)$$

Let c_i be the cost per unit mass for material M_i and C be the maximum allowable material cost. Assuming length as fixed, Eq. (30) can be expressed as

$$\text{area} \times c_i \times \rho_i < C \qquad\qquad (31)$$

And in terms of shape transformers and envelope multipliers, the above constraint reduces to,

$$\Psi_A u v c_i \rho_i < C \qquad\qquad (32)$$

Eq. (32) represents a design constraint that can be plotted in the first quadrant of the four-quadrant-performance chart. Likewise by following the procedure explained in Section 3, different constraints can be plotted in the other three quadrants. For instance, consider the example of the rod design (Section 5.1) where the geometric constraint was expressed by Eq. (29). Two constraints, i.e. torsional constraint and geometric constraint, can be plotted in the first quadrant of Fig. 11. The projections of the relevant points from the decision space to the third quadrant provide solutions in the objective space. Each point of the green[1] bubbles represents a candidate solution satisfying the prescribed set of constraints. Visualized in red, the Pareto frontier is the envelope of all non-dominated solutions. The solutions lying either on or near the Pareto front offer the best compromise as opposed to the others. Fig. 11 shows that only three combinations of shapes and materials can meet the prescribed design constraints. Among them, steel-ellipse is the optimal choice if the designer decides a posteriori to assign an approximate equal weight to both the objective functions. Obviously, other preference would lead to different optimal trade-off. Finally, to determine the final cross-section details, e.g. size, the projections of the optimum trade-off points in the third quadrant can be traced back to the first quadrant. Similarly, a designer can impose any additional constraints in the design variable space and assess their impact on the Pareto front of the objective function space.

6. Conclusion

In this paper, the method of shape transformers has been used to formulate performance indices and develop design maps for the co-selection of shape, size and material in single and multi-objective design. The proposed scheme has been exemplified by considering the case of torsional stiffness design. Formulated for torsional stiffness requirement, the shape transformers have been used to generate multiple performance charts that help visualize the performances of different shapes. It has been shown that shape transformers allow capture the efficiency limits that different combinations of shape and material can achieve. From a comparison of open- and close-walled cross-sections, it appears that the latter are in average 1000 times stiffer than the former. The maps also show that for a fixed envelope, a hollow rectangular shape is more efficient than a hollow circular cross-section in torsional stiffness design. However, the results are different for other geometric constraints.

The method of shape transformers has also been extended to deal with multi-criteria selection of material, shape, and size. In general, the main challenge of multi-criteria selection methods is the ability to visualize simultaneously both the decision space and objective space. We have achieved this by proposing a four-quadrant-performance-chart that systematically establishes a visual relation between design variables and objective function spaces. This method is particularly suitable at the concept stage of design where numerical methods may prevent the user from visualizing and gaining insight into optimal trade-off among design alternatives. Finally, the mathematical model used to formulate the performance indices gives results that are 5% below those obtained with finite element analysis and are, thus, acceptable for the preliminary stage of design.

Appendix A. Formulation of the performance index for mass in torsion stiffness design

Let P_0 be the performance index (mass) for the reference cross-section (solid square). Then, the performance index, P_1 for any arbitrary cross-section with respect to a reference cross-section can be written as

$$\frac{P_1}{P_0} = \frac{m_0}{m_1} = \underbrace{\frac{\rho_0}{\rho_1}}_{\text{Material}} \underbrace{\frac{A_0}{A_1}}_{\text{Geometry}} \qquad\qquad (33)$$

In terms of shape transformers and envelope multipliers, it can be expressed as

$$\frac{P_1}{P_0} = \frac{\rho_0}{\rho_1} \frac{A_0}{A_1} = \frac{\rho_0}{\rho_1} \left(\frac{1}{\Psi_A} \frac{1}{uv} \right) \qquad\qquad (34)$$

Also, the ratio of the torsional stiffness of two cross-sections can be expressed in terms of Shape transformers;

$$\frac{J_{T1}}{J_{T0}} = \left(\frac{J_{T1}}{J_{TD1}} \right) \left(\frac{J_{TD1}}{J_{T0}} \right) = \Psi_{JT1} \left(\frac{J_{TD1}}{J_{TD0}} \right) \qquad\qquad (35)$$

where J_{TD1} is the torsional constant of the rectangular envelope which encloses the shape of cross-section, J_{TD0} is the torsional constant of the reference cross-section. Since the shape and the envelope of a solid square are the same, J_{T0} is equal to J_{TD0}. The ratio of J_{T1}/J_{TD1} is the shape transformer for torsion and J_{TD1}/J_{TD0} represents the effect of scaling.

According to Roark's stress and strain formulas [18], the torsional stiffness of a rectangular cross-section is given by

$$J_{TD} = \frac{BH^3}{16} \left(\frac{16}{3} - 3.36 \frac{H}{B} + 0.28 \left(\frac{H}{B} \right)^5 \right) \qquad\qquad (36)$$

where B and H are the width and the height of the rectangle, respectively. The ratio of torsional constants of two envelopes expressed

by Eq. (36) is not a handy formula. Thus to simplify the formulation, we resort on the method of shape transformers in bending, where the second moment of area is expressed as a product of B and H, i.e. $I = f(BH^3)$; here, we would aim at finding an analogous expression, which will ease the derivation of the performance index. Similar to the bending case, such a function is searched to be of the type

$$J_{TD} = f(B, H) = aB^{b_1}H^{b_2} \tag{37}$$

where a, b_1, and b_2 are the variables to be calculated. The maximum error between the original and approximate function should be less than 5%. Optimum values of a, b_1, and b_2 to minimize the error between Eqs. (36) and (37) has been found by formulating a minimization error problem which will yield the following expression

$$J_{TD} = (0.15)B^{1.55}H^{2.45} \tag{38}$$

Using Eq. (38) and the definition of the envelope multipliers u and v, the relative torsional constant of two envelopes, J_{TD1}/J_{TD0}, is given by

$$\frac{J_{TD1}}{J_{TD0}} = \left(\frac{B_1}{B_0}\right)^{1.55}\left(\frac{H_1}{H_0}\right)^{2.45} = u^{1.55}v^{2.45} \tag{39}$$

Thus, Eq. (35) can be expressed as,

$$\frac{J_{T1}}{J_{T0}} = \left(\frac{J_{T1}}{J_{TD1}}\right)\left(\frac{J_{TD1}}{J_{TD0}}\right) = \Psi_{JT}(u^{1.55}v^{2.45}) \tag{40}$$

Combining the stiffness requirement, i.e. $J_{T0}G_0 = J_{T1}G_1$, and Eq. (40) gives

$$\frac{G_0}{G_1} = \frac{J_{T1}}{J_{T0}} = \left(\frac{J_{T1}}{J_{TD1}}\right)\left(\frac{J_{TD1}}{J_{TD0}}\right) = \Psi_{JT}(u^{1.55}v^{2.45}) \tag{41}$$

Rearranging the terms, the torsional stiffness constraint can be written as

$$\left(\frac{1}{\Psi_{JT}}\frac{G_0}{G_1}\right) = (u^{1.55}v^{2.45}) \tag{42}$$

Based on Eq. (42), the envelope multipliers, u and v, can be found,

$$u = \left(\frac{1}{\Psi_{JT}}\frac{G_0}{G_1}\right)^{\alpha}, v = \left(\frac{1}{\Psi_{JT}}\frac{G_0}{G_1}\right)^{\beta} \tag{43}$$

where

$$1.55\alpha + 2.45\beta = 1 \tag{44}$$

Finally, the ratio of performance indices can be stated as,

$$\frac{P_1}{P_0} = \frac{m_0}{m_1} = \frac{\rho_0}{\rho_1}\frac{1}{\Psi_A}\left(\frac{1}{uv}\right) = \frac{\rho_0}{\rho_1}\frac{1}{\Psi_A}\frac{1}{\left(\frac{1}{\Psi_{JT}}\frac{G_0}{G_1}\right)^{\alpha+\beta}}$$
$$= \frac{\rho_0}{\rho_1}\frac{\Psi_{A0}}{\Psi_{A1}}\left(\frac{\Psi_{JT1}G_1}{\Psi_{JT0}G_0}\right)^{\alpha+\beta} \tag{45}$$

where α and β are obtained by taking natural logarithm from both sides of Eq. (43), and are given by,

$$\alpha = \ln_{(u^{1.55}v^{2.45})}(u), \quad \beta = \ln_{(u^{1.55}v^{2.45})}(v) \tag{46}$$

The "$\alpha + \beta$" term in Eq. (45) is referred to as the scaling parameter, q. Using Eq. (43), the scaling parameter, q, can be expressed in terms of envelope multipliers, u and v, as

$$q = \alpha + \beta = \ln_{(u^{1.55}v^{2.45})}(uv) = \frac{\ln(uv)}{\ln(u^{1.55}v^{2.45})} \tag{47}$$

Hence, a unique performance index can be assigned to each cross-section, and can be expressed in terms of material, shape, and size properties as,

$$P = \frac{1}{m} = \frac{(\psi_{JT}G)^q}{\psi_A\rho} \tag{48}$$

References

[1] Haftka RT, Grandhi RV. Structural shape optimization – a survey. Comput Methods Appl Mech Eng 1986;57(1):91–106.
[2] Kumar AV. A sequential optimization algorithm using logarithmic barriers: applications to structural optimization. J Mech Des, Trans ASME 2000;122(3): 271–7.
[3] Saitou K, Izui K, Nishiwaki S, Papalambros P. A survey of structural optimization in mechanical product development. J Comput Inform Sci Eng 2005;5(3):214–26.
[4] Ghiasi H, Pasini D, Lessard L. Review paper optimum stacking sequence design of composite materials. Part1: constant stiffness design. J Compos Struct 2009;90(1):1.
[5] Shanley FR. Weight–strength analysis of aircraft structures. New York: Dover; 1960.
[6] Cox HL. The design of structures of least weight, international series of monographs in aeronautics and astronautics. Oxford: Pergamon Press; 1965.
[7] Parkhouse JG. Structuring: a process of material dilution. In: Proceedings of the 3rd International Conference on Space Structures; 1984. p. 367–74.
[8] Ashby MF. Materials selection in conceptual design. Mater Sci Technol 1989;5(6):517–25.
[9] Ashby MF. Overview no. 92 materials and shape. Acta Metall Mater 1991;39(6):1025–39.
[10] Weaver PM, Ashby MF. The optimal selection of material and section-shape. J Eng Des 1996;7(2):129–50.
[11] Hunag JS, Gibson LJ. Materials and cross-sectional shapes for bending stiffness. Mater Sci Eng 1993;163(1):51–9.
[12] Rakshit S, Ananthasuresh GK. Simultaneous geometry optimization and material selection for truss structures. In: ASME Conference on proceedings: 32nd design automation conference, Philadelphia, PA, vol. 1; 2006. p. 629–38.
[13] Wanner A. Minimum-weight materials selection for limited available space. J Mater Des 2010;31(6):2824–39.
[14] Thomas P, Qidwai MA. Mechanical design and performance of composite multifunctional materials. Acta Mater 2004;52(8):2155–64.
[15] Amany A, Pasini D. Shape and material selection for optimizing structural performance in bending and shear stiffness design. J Mater Des 2007;30:1633–42.
[16] Pasini D. Shape transformers for material and shape selection of lightweight beams. J Mater Des 2006;28(7):2071–9.
[17] Pasini D. Shape and material selection for optimizing flexural vibrations in multilayered resonators. IEEE 2006;15(6):1745–58.
[18] Young WC, Budynas RG, Roark RJ. Roark's formulas for stress and strain, formulas for stress and strain. New York: McGraw-Hill; 2002.
[19] Ashby MF. Materials selection in mechanical design. Oxford: Elsevier Butterworth–Heinemann; 2005.
[20] Trahair NS. Nonlinear elastic nonuniform torsion. J Struct Eng 2005;131(7): 1135–42.
[21] Pasini D, Smith DJ, Burgess SC. Structural efficiency maps for beams subjected to bending. Proceedings of the institution of mechanical engineers. Part L: J Mater: Des Appl 2003;217(3):207–20.
[22] Deb K. Multi-objective optimization using evolutionary algorithms. West Sussex: John Wiley & sons; 2001.